Available online at www.sciencedirect.com
ScienceDirect
Ceramics International 35 (2009) 3435–3440
CERAMICS INTERNATIONAL
www.elsevier.com/locate/ceramint

Preparation and varistor properties of new quaternary Zn–V–Mn–(La, Dy) ceramics

Choon-W. Nahm *

Semiconductor Ceramics Lab., Department of Electrical Engineering, Dongeui University, Busan 614-714, Republic of Korea

Received 20 April 2009; received in revised form 15 May 2009; accepted 12 June 2009
Available online 7 July 2009

Abstract

The La and Dy doping effects on microstructures, nonlinear electrical properties, and its stability of ZVM (Zn–V–Mn)-based ceramics were investigated. The microstructure of the quaternary ZVML (Zn–V–Mn–La)-based ceramics doped with La and quaternary ZVMD (Zn–V–Mn–Dy)-based ceramics doped with Dy commonly consisted of mainly ZnO grains and $Zn_3(VO_4)_2$ as a secondary phase. In addition, the quaternary ZVML- and ZVMD-based ceramics revealed the secondary phases, such as $LaVO_4$ and $DyVO_4$, respectively, in addition to $Zn_3(VO_4)_2$. It seems that all secondary phases act as a liquid-phase sintering aid because it has a significant effect on the sintered density and average grain size. The incorporation of La and Dy into the ZVM-based ceramics increased the breakdown field, and improved the nonlinear electrical properties, in which the nonlinear coefficient was close to 33. The ZVML-based ceramics exhibited the best stability, where the variation of breakdown field ($\%\Delta E_B$) against DC accelerated aging stress is −9.7%.

Keywords: C. Electrical properties; Microstructure; Quaternary-based varistors; Varistor ceramics

1. Introduction

Pure ZnO exhibits ohmicity through a sintering process, whereas ZnO ceramics doped with minor metal oxides exhibit remarkable nonohmicity. Microstructurally, they are comprised of semiconducting n-type ZnO grains, which are surrounded by insulating intergranular layers at grain boundaries. Electrically, they show highly nonlinear current–voltage characteristics similar to the back-to-back Zener diode, but with much greater voltage, current, and energy handling capabilities [1,2]. Thus, they, called varistors, are commonly used as ESD (electrostatic discharge) and surge absorbers in electronic circuits.

ZnO ceramics cannot exhibit a nonlinear behavior without adding heavy elements with large ionic radii, such as Bi, Pr, Ba, etc. Commercial ZnO–Bi_2O_3-based ceramics and ZnO–Pr_6O_{11}-based ceramics cannot be co-fired with a silver inner-electrode (m.p. 961 °C) in multilayered chip components because of the relatively high sintering temperature [3,4]. Therefore, new nonlinear ceramics are required in order to use a silver inner-electrode. Among the various ceramics, one candidate is the binary ZnO–V_2O_5 (ZV)-based ceramics [5–9]. This ZV-based ceramics can be sintered at relatively low temperature in the vicinity of about 900 °C. This is important for multilayer chip component applications, because it can be co-sintered with a silver inner-electrode without using expensive palladium or platinum metals. The ZV-based ceramics have been studied for ternary ceramics containing Mn mainly up to now [10–16]. To develop the nonlinearity of high performance for ternary ZVM (Zn–V–Mn)-based ceramics, it is very important to comprehend the influences of new additives on nonlinear electrical properties. The La and Dy are often added to ZnO–Pr_6O_{11}-based ceramics to improve the nonlinear electrical properties [3,4]. No study of the effects of La and Dy on the varistor properties in ternary ZVM-based ceramics has been reported, especially, on the stability against DC accelerated aging stress.

This paper reports microstructure, varistor properties, and its stability of the ternary ZVM (Zn–V–Mn)-based ceramics doped with La (ZVML) and ZVM-based ceramics doped with Dy (ZVMD) and some new results were obtained.

* Tel.: +82 51 890 1669; fax: +82 51 890 1664.
E-mail address: cwnahm@deu.ac.kr.

0272-8842/$36.00
doi:10.1016/j.ceramint.2009.06.004

2. Experimental procedure

2.1. Sample preparation

Reagent-grade raw materials were used in the proportions of 98.75 mol% ZnO, 0.5 mol% V_2O_5, 0.5 mol% Mn_3O_4, and independent samples La_2O_3 and Dy_2O_3 of 0.25 mol%. Raw materials were mixed by ball milling with zirconia balls and acetone in a polypropylene bottle for 24 h. The mixture was dried at 120 °C for 12 h. The dried mixture was mixed into a container with acetone and 0.8 wt% polyvinyl butyral (PVB) binder of powder weight. After drying at 120 °C for 24 h, the mixture was granulated by sieving through a 100-mesh screen to produce starting powder. The powder was uniaxially pressed into discs of 10 mm in diameter and 1.5 mm in thickness at a pressure of 80 MPa. The discs were sintered at 900 °C in air for 3 h and furnace cooled to room temperature. The final samples were about 8 mm in diameter and 1.0 mm in thickness. Silver paste was coated on both faces of the samples and the ohmic contacts were formed by heating at 600 °C for 10 min. The electrodes were 5 mm in diameter.

2.2. Microstructure analysis

Both surfaces of the samples were lapped and ground with SiC paper and polished with 0.3-μm Al_2O_3 powder to a mirror-like surface. The polished samples were chemically etched into $1HClO_4$:$1000H_2O$ for 40 s at room temperature. The surface of the samples was metallized with a thin coating of Au to reduce charging effects and to improve the resolution of the image. The surface microstructure was examined by scanning electron microscopy (SEM, Model S2400, Hitachi, Japan). The average grain size (d) was determined by the linear intercept method [17]. The compositional analysis of the selected areas was determined by an attached energy dispersion X-ray analysis (EDX). The crystalline phases were identified by powder X-ray diffraction (XRD, Model D/max 2100, Rigaku, Japan) with Ni filtered CuK_α radiation. The sintered density (ρ) was measured by the Archimedes method.

2.3. Electrical measurement

The E–J characteristics of the samples were measured using an I-V meter (Keithley 237 SMU). The breakdown field (E_B) was measured at 1.0 mA cm^{-2} and the leakage current density (J_L) was measured at 0.8 E_B. In addition, the nonlinear coefficient (α) is defined by the empirical law, $J = KE^{\alpha}$, where J is the current density, E is the applied electric field, and K is a constant. The α was determined in the current density range 1.0–10 mA cm^{-2}, where $\alpha = 1/(\log E_2 - \log E_1)$, and E_1 and E_2 are the electric fields corresponding to 1.0 mA cm^{-2} and 10 mA cm^{-2}, respectively. The DC accelerated aging test was performed for a stress state of 0.85 E_B/85 °C/24 h. The degradation rate coefficient (K_T) was calculated from the expression $I_L = I_{Lo} + K_T t^{1/2}$ [18], where I_L is the leakage current at stress time (t) and I_{Lo} is I_L at $t = 0$. After applying the respective stresses, the I–V characteristics were measured at room temperature. Five samples (with the same composition) were used for all electrical measurements and the average value was obtained.

3. Results and discussion

3.1. Phase composition and microstructure

Fig. 1 shows the SEM images of the samples. It can be seen that the grain structure of the ZVM sample is very

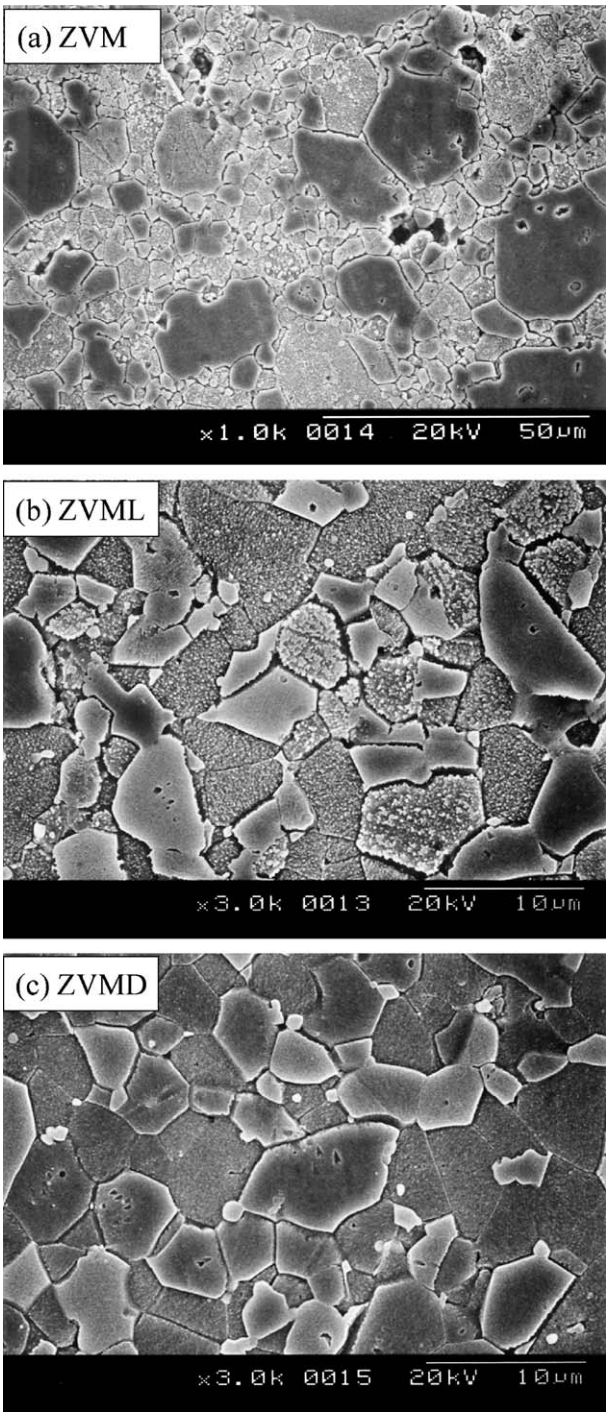

Fig. 1. SEM micrographs of the ZVM-based ceramics doped with La and Dy.

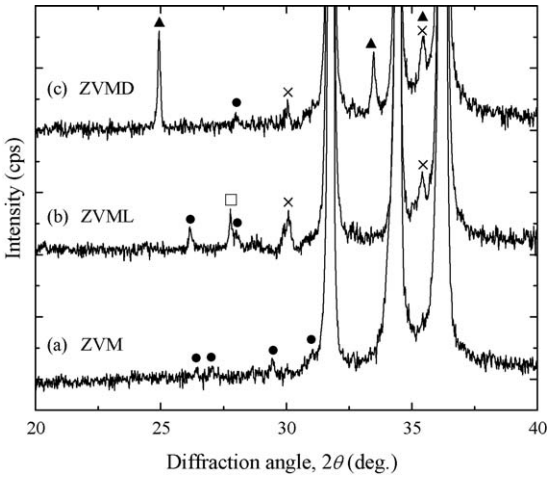

Fig. 2. XRD patterns of the ZVM-based ceramics doped with La and Dy; (●): $Zn_3(VO_4)_2$; (□): $LaVO_4$; (▲): $DyVO_4$; (×): Mn-rich phase (Mn_3O_4).

heterogeneously distributed throughout the samples. The ZVM sample showed very abnormal grain growth of the ZnO. On the contrary, the ZVML and ZVMD samples were remarkably uniformed in the grain size, compared with the ZVM sample. Therefore, the incorporation of La and Dy effectively reduced the abnormal grain growth. It assumed that this is attributed to the restriction of abnormal ZnO grain growth due to the secondary phase generated by La and Dy doping. Uniform grain is very important in varistor application, because it prevents the concentration of current flowing through grains. The average grain sizes of the ZVM, ZVML, and ZVMD samples exhibited 5.2 μm, 8.4 μm, and 7.4 μm, respectively. The sintered densities of the ZVM, ZVML, and ZVMD samples were in the range of 95.3%, 95.5%, and 96.4% of theoretical density (TD) (theoretical density 5.78 g cm^{-3} for ZnO). La and Dy slightly improved the sintered density. This has a significant effect on the improvement of electrical stability. The XRD patterns of the samples are shown in Fig. 2. The XRD patterns in all the samples revealed the presence of $Zn_3(VO_4)_2$ as a secondary phase, in addition to a primary phase of hexagonal ZnO. In addition, the ZVML and ZVMD samples revealed the presence of $LaVO_4$ and $DyVO_4$ as the secondary phases, respectively. The $Zn_3(VO_4)_2$ is formed when the ZV-based ceramics are sintered at high temperatures and that acts as a liquid-phase sintering aid [5]. Furthermore, it seems that $LaVO_4$ and $DyVO_4$ act as an enhancer for the grain growth of ZnO, in the light of experimental results. No secondary phase related to Mn was detected. The EDX microanalysis for the samples doped with La and Dy is shown in Fig. 3. No peak for the V-species is found in the grain interior within an EDX detection limit, though the ion radius of V is smaller than that of Zn. This means the V-species is not dissolved into the ZnO grain. However, the Mn-species was found to exist at the grain interior, in addition to Zn. On the other hand, it was found that the grain boundaries (GB) contain V- and Mn-species. As a result, the Mn-species exist in both grain and grain boundaries. It can be seen from Fig. 3(c) and (d) that La and Dy are segregated to grain boundaries because the ionic radius of La^{3+}

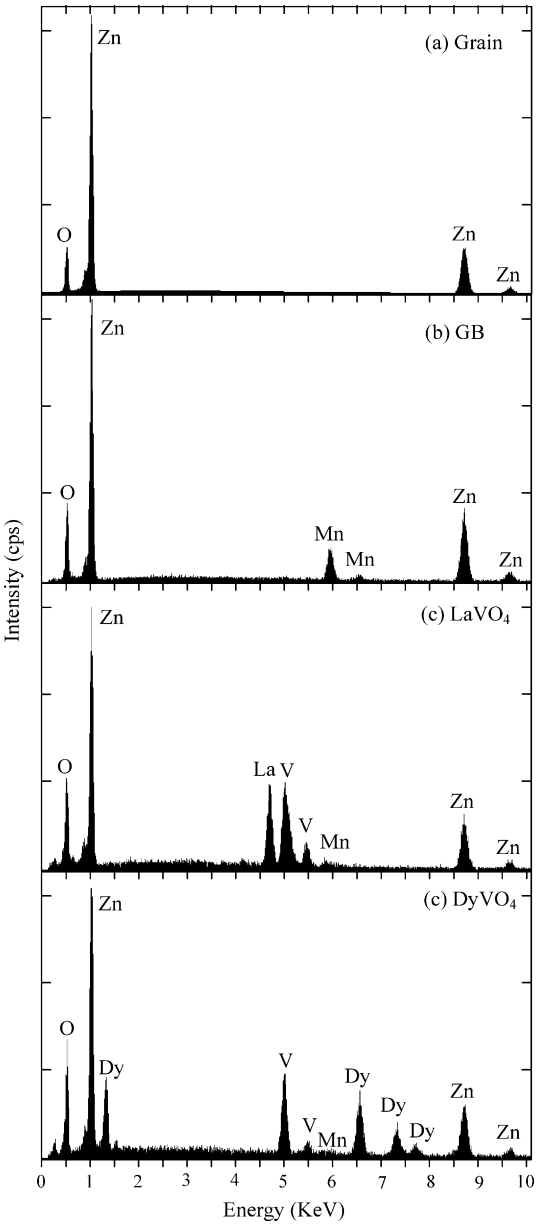

Fig. 3. EDX analysis of the ZVM-based ceramics doped with La and Dy.

and Dy^{3+} are larger than that of Zn^{2+}. Presumably, this ion migration will have an effect on electrical properties.

3.2. Electrical properties

Fig. 4 shows the electric field-current density (*E–J*) characteristics of the ZVM sample doped with La and Dy. The *E–J* characteristics of the samples are characterized by the nonlinearity. The curves show that the conduction characteristics divide into two regions: an ohmic region with very high impedance before the breakdown field and a nonlinear region with very low impedance after the breakdown field. All of the samples show similar curves, except for the breakdown field.

Fig. 5 compares the breakdown field (E_B) and nonlinear coefficient (α) with additives. The E_B of ZVM sample was

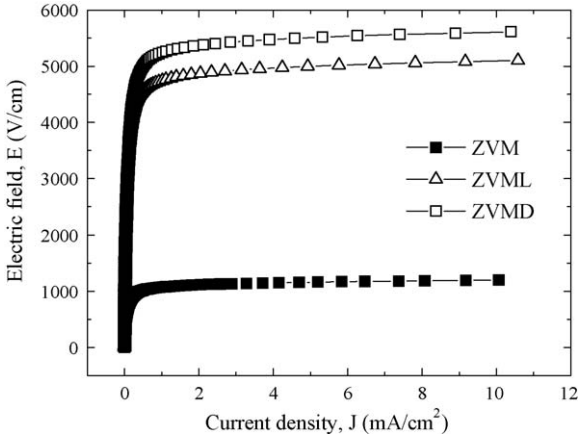

Fig. 4. *E–J* characteristics of the ZVM-based ceramics doped with La and Dy.

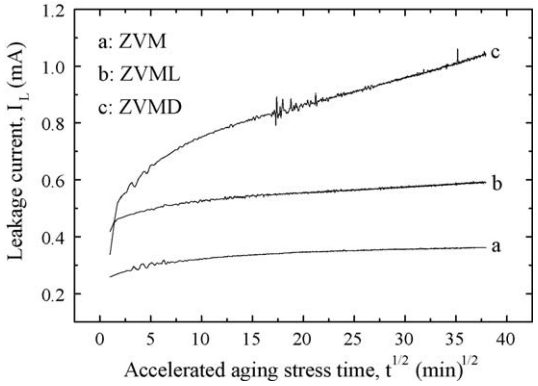

Fig. 6. Leakage current during DC accelerated aging stress of the ZVM-based ceramics doped with La and Dy.

1106 V cm^{-1}. However, the breakdown field of the ZVML and ZVMD samples greatly increased to 4804 V cm^{-1} and 5287 V cm^{-1}, respectively. In general, the E_B is firstly affected by the number of grain boundaries (n) across a series between the electrodes, which is inversely proportional to the average grain size. As a result, the decrease of the grain size leads to higher E_B. The E_B is secondly affected by the breakdown voltage per grain boundaries (v_{gb}), as expressed by the following equation [1]; $E_B = v_{gb}/d$, where d is the grain size. As a result, the increase of the v_{gb} leads to higher E_B. It is forecasted that the increase of average grain size with impurity doping will decrease the E_B. However, this is opposite to experimental results. If so, it is assumed that the increase of E_B in the ZVML and ZVMD samples is attributed to the increase of the v_{gb}, compared with the ZVM sample. The v_{gb} was in the range of 3.9–4.0 V/gb for the doped samples. It is also interesting to note that the doped samples exhibited a general value of 2–4 V/gb [1]. This suggests that the grain boundaries have the active electronic states. Therefore, the increase of E_B with impurity doping could be agreed to be due to the increase of v_{gb} rather than the effect of grain size.

The ZVM sample exhibited high nonlinear properties by presenting 22 in the nonlinear coefficient (α), compared with α = 13–18 for well-known ternary Zn–Bi–Co-based ceramics or Zn–Bi–Mn-based ceramics. Furthermore, the ZVML and ZVMD samples exhibited α = 33. Therefore, it can be seen that La and Dy are significant dopants, which greatly improve the nonlinear properties. This results from a more activated grain boundary by the migration of La and Dy ions toward the grain boundary. The leakage current density (J_L) of the ZVM sample was about 0.22 mA cm^{-2}, whereas the J_L value of the ZVML and ZVMD samples decreased to 0.16 mA cm^{-2} and 0.17 mA cm^{-2}, respectively. This has a significant effect on the improvement of electrical stability together with sintered density, as mentioned previously. Incorporation of La and Dy to the ZVM sample remarkably improves the nonlinear properties, resulting in higher nonlinear coefficient and smaller leakage current. It is presumed that the incorporation of La and Dy to the ZVM sample enhances the electronic activity of grain boundaries; raising potential barrier height at grain boundaries.

3.3. DC accelerated aging characteristics

Fig. 6 shows the variation of leakage current during the DC accelerated aging stress of the ZVM sample doped with La and Dy. The leakage current (I_L) increased in order of

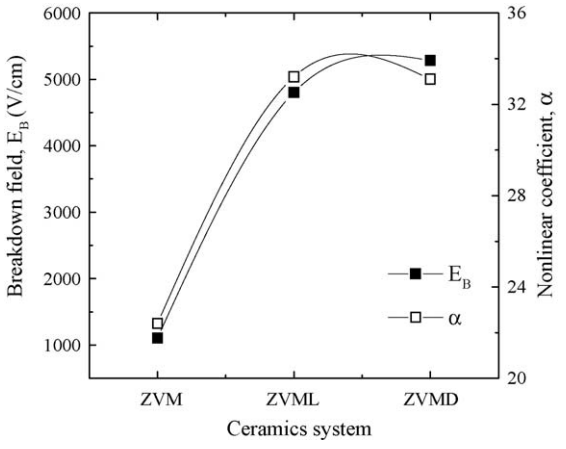

Fig. 5. Breakdown field and nonlinear coefficient of the ZVM-based ceramics doped with La and Dy.

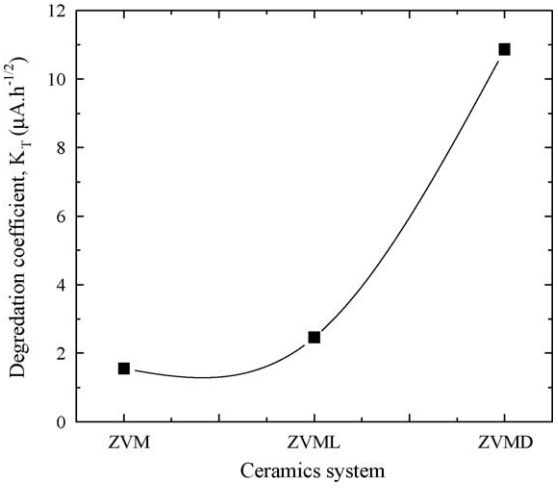

Fig. 7. Degradation coefficient of the ZVM-based ceramics doped with La and Dy.

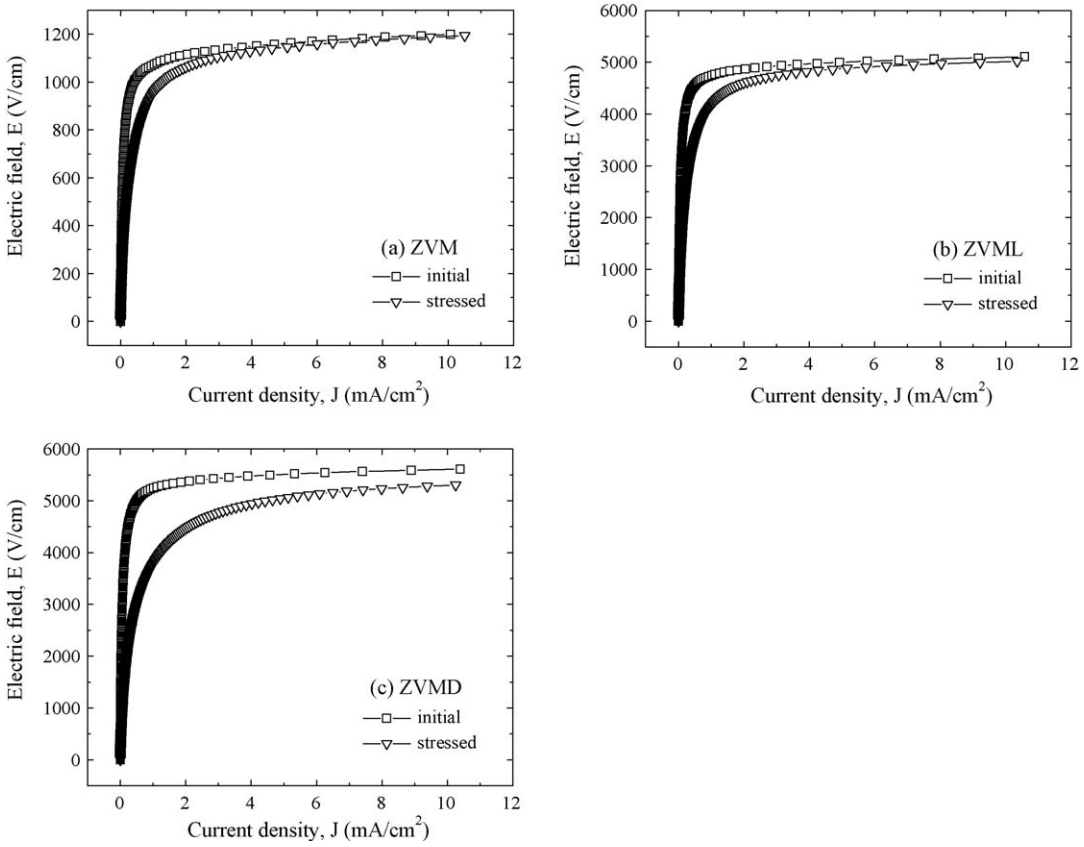

Fig. 8. *E–J* characteristic behavior after DC accelerated aging stress of the ZVM-based ceramics doped with La and Dy.

ZVM → ZVML → ZVMD (I_L: ZVM < ZVML < ZVMD) during DC accelerated aging stress. On the whole, all of the samples exhibited high stability without thermal runaway. The stability for nonlinear properties of the samples can be estimated by the degradation rate coefficient (K_T), indicating the degree of aging. The K_T value of the samples is shown in Fig. 7. The ZVM sample exhibited weak positive creep of leakage current (PCLC), with K_T values of +1.55 μA h$^{-1/2}$. However, the ZVML and ZVMD samples exhibited strong PCLC with the K_T value of +2.46 and +10.86 μA h$^{-1/2}$, respectively. Though the leakage current and sintered density of doped samples are better than those of the ZVM sample, the low stability is likely to be related to $LaVO_4$ and $ZnVO_4$ as a secondary phase, which decrease cross-sectional area of grain boundary. This decrease of cross-sectional area leads to the concentration of current in the conduction path. The *E–J* characteristic behavior before and after DC accelerated aging stress of the ZVM sample doped with La and Dy is shown in Fig. 8. The *E–J* curves of the ZVM and ZVML samples show the large variation in the vicinity of knee than that at low and high field regime after stress. However, the *E–J* curve of the ZVMD sample shows the larger variation than that of the ZVM and ZVML samples, in electric field regime more than 1500 V cm^{-1} after applying the stress. When the *E–J* curves shifted toward low electric field after applying the stress, the samples are degraded. For this reason, the ZVMD sample exhibited remarkable degradation, compared with the ZVM and ZVML samples. This coincides with the variation of the K_T value.

Fig. 9 compares the variation of E_B after the stress with initial E_B with the additives. The ZVML sample was less than −10% in $\%\Delta E_B$, exhibiting higher stability than the ZVM sample. In contrast, the ZVMD sample exhibited high variation, −25.5% in $\%\Delta E_B$. In the same way, the variation of α after the stress with initial α with the additives is shown in Fig. 10. On the whole, the variation for α of all samples exhibited to be high, unlike the breakdown field (E_B). Of the samples, the ZVM

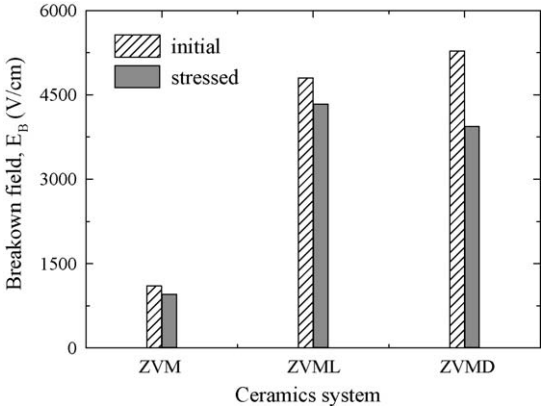

Fig. 9. Breakdown field before and after DC accelerated aging stress of the ZVM-based ceramics doped with La and Dy.

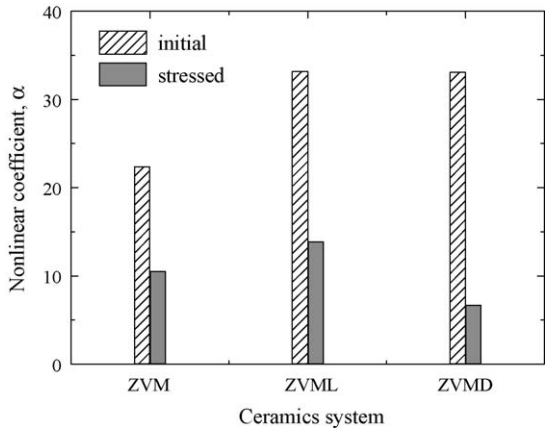

Fig. 10. Nonlinear coefficient before and after DC accelerated aging stress of the ZVM-based ceramics doped with La and Dy.

sample undoped with La and Dy exhibited the least variation rate against DC accelerated aging stress.

4. Conclusions

The microstructure of the ZVM-based ceramics doped with Dy and La commonly consisted of main phase of the ZnO grains and $Zn_3(VO_4)_2$ as a secondary phase. Furthermore, in addition to $Zn_3(VO_4)_2$, the quaternary La-doped ZVM (ZVML) and Dy-doped ZVM (ZVMD)-based ceramics were found to possess a secondary phase, such as $LaVO_4$ and $DyVO_4$, respectively. It seems that all secondary phases act as a liquid-phase sintering aid because it has a significant effect on the sintered density and the average grain size. The La and Dy as a dopant greatly improved the nonlinear electrical properties of the ZVM-based ceramics, in which the nonlinear coefficient (α) is about 33 and the leakage current density is close to 16 $\mu A\,cm^{-2}$. The ZVML-based ceramics exhibited the best stability, which the variation of breakdown field ($\%\Delta E_B$) against DC accelerated aging stress is -9.7%. Conclusively, it is estimated that ZVML-based ceramics could be sufficiently applied as a useful material for multilayer chip varistors with an Ag inner-electrode.

References

[1] L.M. Levinson, H.R. Philipp, Zinc oxide varistor—a review, Am. Ceram. Soc. Bull. 65 (1986) 639–646.
[2] T.K. Gupta, Application of zinc oxide varistor, J. Am. Ceram. Soc. 73 (1990) 1817–1840.
[3] C.-W. Nahm, C.-H. Park, H.-S. Yoon, Highly stable nonohmic characteristics of ZnO–Pr_6O_{11}–CoO–Dy_2O_3 based varistors, J. Mater. Sci. Lett. 19 (2000) 725–727.
[4] C.-W. Nahm, Influence of La_2O_3 additives on microstructure and electrical properties of ZnO–Pr_6O_{11}–CoO–Cr_2O_3–La_2O_3-based varistors, Mater. Lett. 59 (2005) 2097–2100.
[5] J.-K. Tsai, T.-B. Wu, Non-ohmic characteristics of ZnO–V_2O_5 ceramics, J. Appl. Phys. 76 (1994) 4817–4822.
[6] J.-K. Tsai, T.-B. Wu, Microstructure and nonohmic properties of binary ZnO–V_2O_5 ceramics sintered at 900 °C, Mater. Lett. 26 (1996) 199–203.
[7] C.T. Kuo, C.S. Chen, I.-N. Lin, Microstructure and nonlinear properties of microwave-sintered ZnO–V_2O_5 varistors: I. Effect of V_2O_5 doping, J. Am. Ceram. Soc. 81 (1998) 2942–2948.
[8] H.-H. Hng, K.M. Knowles, Characterisation of $Zn_3(VO_4)_2$ phases in V_2O_5-doped ZnO varistors, J. Eur. Ceram. Soc. 19 (1999) 721–726.
[9] H.-H. Hng, L. Halim, Grain growth in sintered ZnO–1 mol% V_2O_5 ceramics, Mater. Lett. 57 (2003) 1411–1416.
[10] H.-H. Hng, P.L. Chan, Microstructure and current–voltage characteristics of ZnO–V_2O_5–MnO_2 varistors, Ceram. Int. 30 (2004) 1647–1653.
[11] C.-W. Nahm, Microstructure and electrical properties of vanadium-doped zinc oxide-based non-ohmic resistors, Solid State Commun. 143 (2007) 453–456.
[12] C.-W. Nahm, Improvement of electrical properties of V_2O_5 modified ZnO ceramics by Mn-doping for varistor applications, J. Mater. Sci.: Mater. Electron. 19 (2008) 1023–1029.
[13] C.-W. Nahm, Influence of Mn doping on microstructure and DC-accelerated aging behaviors of ZnO–V_2O_5-based varistors, Mater. Sci. Eng. B 150 (2008) 32–37.
[14] H.-H. Hng, K.Y. Tse, Effects of MgO doping in ZnO–0.5 mol% V_2O_5 varistors, Ceram. Int. 34 (2008) 1153–1157.
[15] H.-H. Hng, P.L. Chan, Cr_2O_3 doping in ZnO–0.5 mol% V_2O_5 varistor ceramics, Ceram. Int. 35 (2009) 409–413.
[16] C.-W. Nahm, Effect of MnO_2 addition on microstructure and electrical properties of ZnO–V_2O_5-based varistor ceramics, Ceram. Int. 35 (2009) 541–546.
[17] J.C. Wurst, J.A. Nelson, Lineal intercept technique for measuring grain size in two-phase polycrystalline ceramics, J. Am. Ceram. Soc. 55 (1972) 109–111.
[18] J. Fan, R. Freer, Deep level transient spectroscopy of zinc oxide varistors doped with aluminum oxide and/or silver oxide, J. Am. Ceram. Soc. 77 (1994) 2663–2668.